Inviscid Channel Flow over a Smooth Bump via Discontinuous Galerkin and Stabilized Petrov-Galerkin methods

Li Wang, W. Kyle Anderson and J. Taylor Erwin
SimCenter: National Center for Computational Engineering
University of Tennessee at Chattanooga, Chattanooga, TN

1. Code description

The current flow solver makes use of high-order discontinuous Galerkin (DG) discretizations with up to fifth-order accuracy (i.e. p = 4). The convective flux on elemental interfaces is resolved by the HLLC Riemann flux function, while the discretization of the viscous flux is based on implementation of a symmetric interior penalty method. To enhance solution efficiency, the solver uses a p-multigrid approach, driven by a linearized element Gauss-Seidel smoother or a Generalized Minimal Residual (GMRES) algorithm. The present high-order discontinuous Galerkin (2D & 3D) solver is capable of using the standard MPI message-passing library for inter-processor communication, where the mesh is partitioned based on the METIS graph partitioner. In addition, curved boundary elements are often required and employed in the solver to accurately represent complex geometries and to improve solution accuracy.

A stabilized Petrov-Galerkin (PG) code has also been developed with accuracy ranging from second order to fourth order (p = 3). The solution is obtained using an approximate Newton method where the linear system is solved using a preconditioned GMRES approach with ILU(k) preconditioning. For higher-order elements, the boundaries are curved to accurately represent the geometry.

2. Case summary

In this benchmark case, the L_2 norm of the density residual is monitored and the residual tolerance is set to be 10^{-12}. All the mesh and order refinement studies are performed on a single processor, where the average Taubench CPU time is 8.8464 seconds.

3. Meshes

A sequence of four unstructured meshes, containing 515, 2060, 8240 and 32960 triangular elements, are used in this case for the accuracy and efficiency study. The computational domain is bounded between x = -1.5 and x = 1.5, and between the bump and y = 0.8. Inviscid wall boundary conditions are set on the top and bottom walls, while subsonic inflow and outflow boundary conditions are specified at the inlet and outlet, respectively. The coarsest mesh is displayed in Fig. 1 and the finer meshes are obtained by sequentially performing 1:4 uniform mesh refinement. To enable the use of high-order curved elements (whose order is set to be consistent with the flow analysis solution), additional bump

surface points are required, which are initially created by linear interpolation of the vertex coordinates and then projected onto the surface of the original geometry.

For the Petrov-Galerkin cases, the meshes differ from those discussed above because they have been generated using a different meshing code. Nevertheless, the meshes used in the PG cases are also unstructured and have similar element counts as those above, with corresponding (triangular) elements of 606, 2406, 9696, and 38,892.

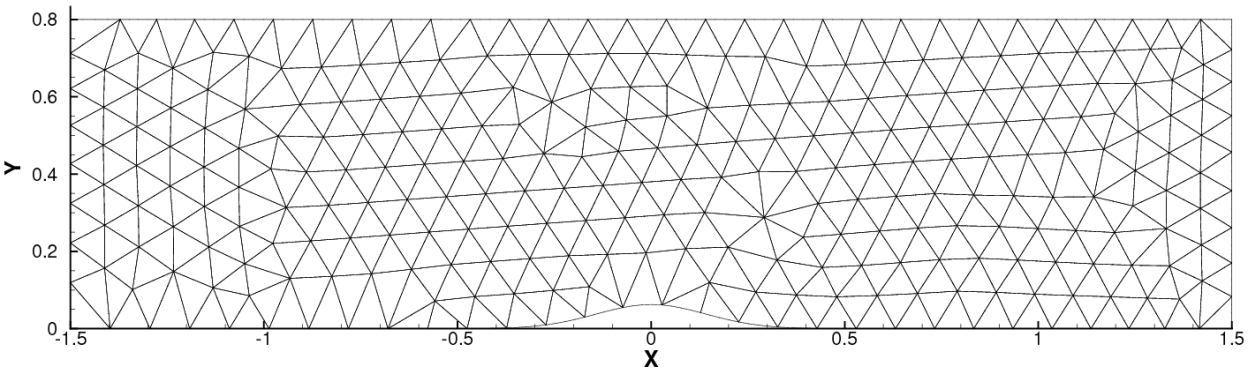

Figure 1. The coarsest unstructured mesh (containing 515 elements and 297 nodes) used in the DG solver for the inviscid bump benchmark test case.

4. Results

The simulation starts with uniform flow with Mach number of 0.5. Various orders of DG discretizations ranging from p = 0 to p = 3 are compared in the results. Fig. 2 displays the steady-state pressure solution obtained by the respective second-order and fourth-order DG discretizations on the coarsest mesh. One can observe that the higher-order scheme delivers a much smoother solution than the low-order scheme even though the mesh is very coarse. Furthermore, due to the nature of inviscid flow with smooth solution, spatial discretization error can be quantified through computation of the generated entropy. Fig. 3 (a) shows the spatial error convergence as a function of length scale defined as $\mathrm{h} = 1/\sqrt{\mathrm{nDoFs}}$, where the slopes of the p = 0, p = 1, p = 2 and p = 3 DG schemes are 0.75, 1.42, 3.02 and 3.82, respectively. Fig. 3 (b) depicts the entropy error convergence in terms of work units (where the computational time is scaled by the TauBench time). It can be concluded that a higher-order DG scheme performs more efficiently than a lower-order scheme to obtain a certain level of solution accuracy.

Results obtained using the stabilized Petrov-Galerkin formulation are shown in Fig. 4. As seen, the error levels are in a similar range as the ones obtained by the DG schemes. In terms of length scale, the asymptotic slopes of the error convergence for p = 1, p = 2, and p = 3 elements are 2.39, 2.77, and 4.03, respectively. In terms of work units as displayed in Fig. 4 (b), the fourth-order stabilized PG scheme performs most efficiently to achieve a certain level of solution accuracy.

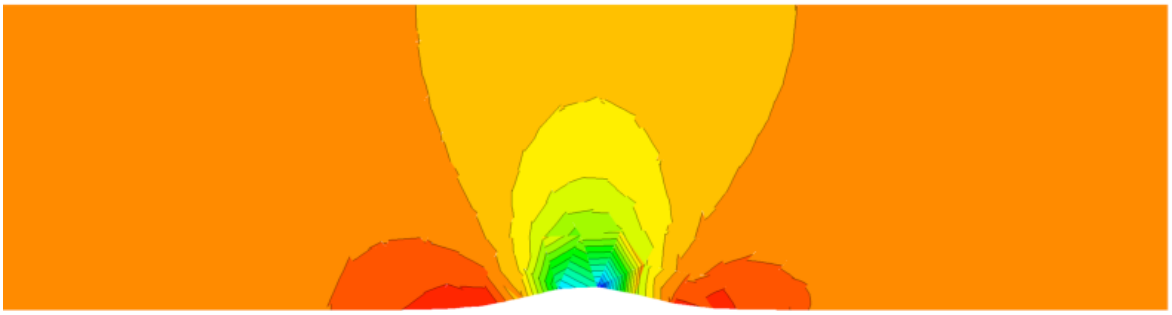

(a) Second-order DG scheme

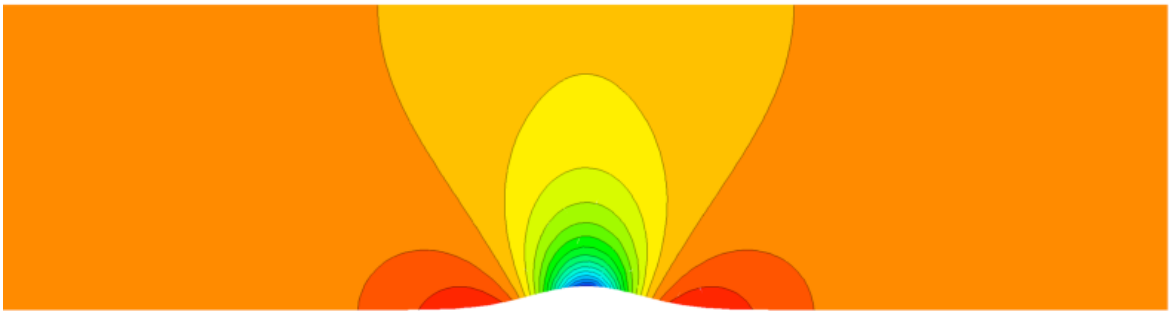

(b) Fourth-order DG scheme

Figure 2. Steady-state pressure contours obtained using second-order (a) and fourth-order (b) DG discretizations on the coarsest mesh.

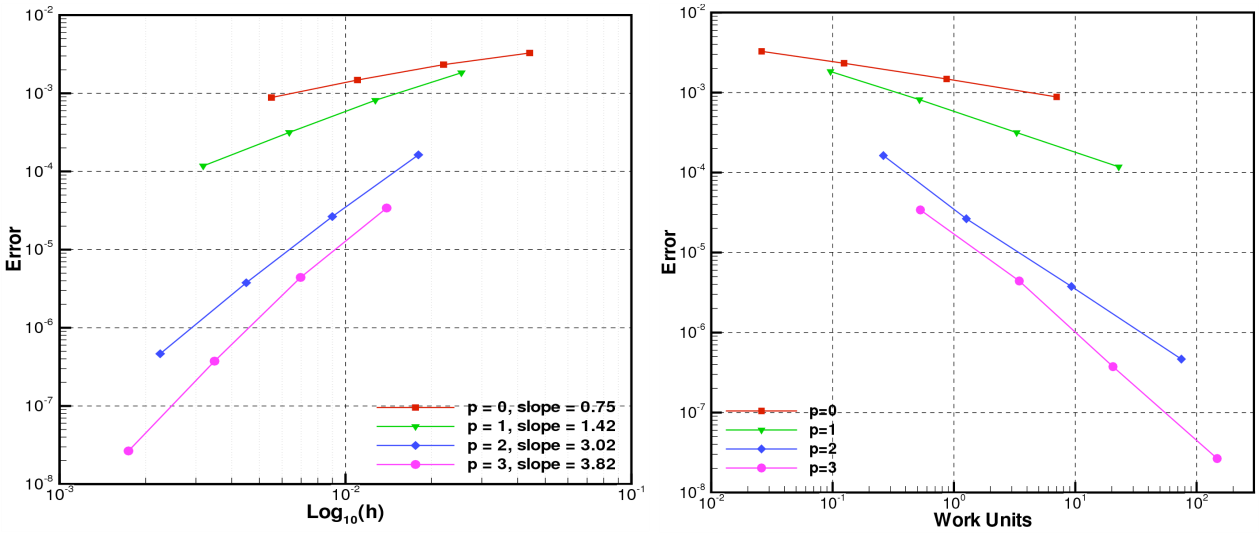

(a) Solution error vs. length scale

(b) Solution error vs. work units

Figure 3. Convergence of the L_2 norm of entropy error for various orders of DG schemes in the inviscid bump case.

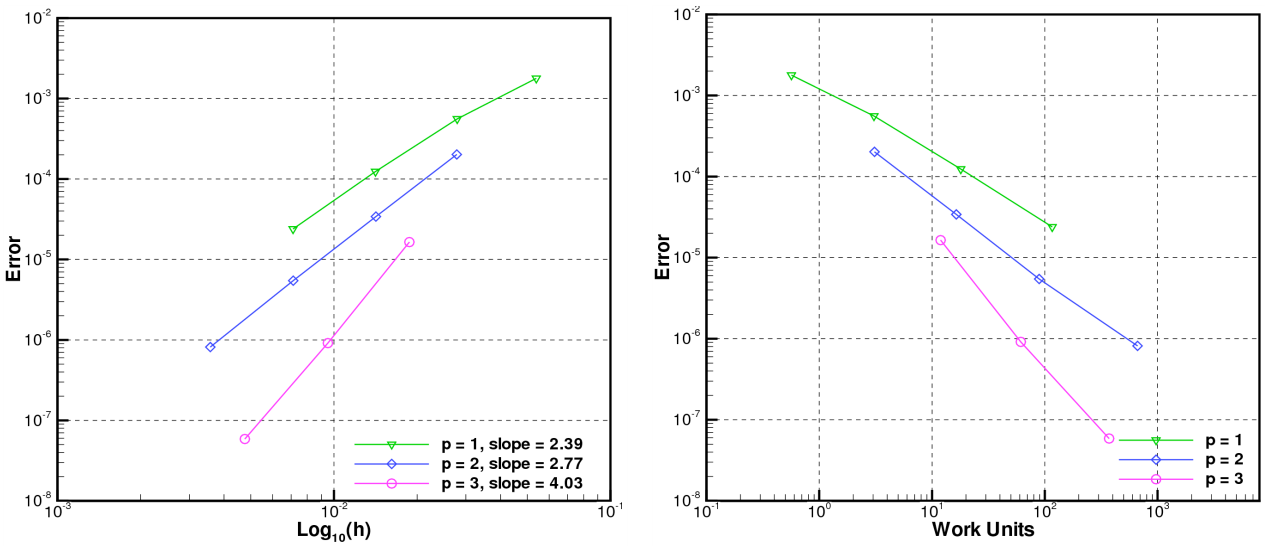

(a) Solution error vs. length scale

(b) Solution error vs. work units

Figure 4. Convergence of the L_2 norm of entropy error for various orders of stabilized Petrov-Galerkin schemes in the inviscid bump case.